Protection and Control of Modern Power Systems

ORIGINAL RESEARCH

Open Access

Dynamic reconfiguration for TEG systems under heterogeneous temperature distribution via adaptive coordinated seeker

Yijun Chen[1], Bo Yang[1*], Zhengxun Guo[1], Jingbo Wang[1], Mengmeng Zhu[2], Zilin Li[3] and Tao Yu[4]

Abstract

A thermoelectric generation (TEG) system has the weakness of relatively low thermoelectric conversion efficiency caused by heterogeneous temperature distribution (HgTD). Dynamic reconfiguration is an effective technique to improve its overall energy efficiency under HgTD. Nevertheless, numerous combinations of electrical switches make dynamic reconfiguration a complex combinatorial optimization problem. This paper aims to design a novel adaptive coordinated seeker (ACS) based on an optimal configuration strategy for large-scale TEG systems with series–parallel connected modules under HgTDs. To properly balance global exploration and local exploitation, ACS is based on 'divide-and-conquer' parallel computing, which synthetically coordinates the local searching capability of tabu search (TS) and the global searching capability of a pelican optimization algorithm (POA) during iterations. In addition, an equivalent re-optimization strategy for a reconfiguration solution obtained by meta-heuristic algorithms (MhAs) is proposed to reduce redundant switching actions caused by the randomness of MhAs. Two case studies are carried out to assess the feasibility and superiority of ACS in comparison with the artificial bee colony algorithm, ant colony optimization, genetic algorithm, particle swarm optimization, simulated annealing algorithm, TS, and POA. Simulation results indicate that ACS can realize fast and stable dynamic reconfiguration of a TEG system under HgTDs. In addition, RTLAB platform-based hardware-in-the-loop experiments are carried out to further validate the hardware implementation feasibility.

Keywords: Thermoelectric generation systems, Dynamic reconfiguration, Heterogeneous temperature distribution, Adaptive coordinated seeker

1 Introduction

Coinciding with rapid economic growth, over the past few decades, global demand for electrical energy has increased dramatically [1–3]. However, traditional fossil fuels currently acting as the main source of electricity generation, e.g., oil, coal, natural gas [4], face ever-increasing depletion while causing severe environmental deterioration [5]. Hence, it is crucial to reform the current energy structure and utilization patterns. Renewable energy is envisaged as a revolutionary and promising candidate to ease the continued tension and pressure in the global energy crisis [6].

In addition to wind, hydro, solar, and hydrogen [7, 8], thermoelectric generation (TEG) also possesses remarkable application potential and value [9] because of its prominent advantages of simple structure, sturdiness, being noiseless, long service life, etc. TEG has been applied in some industrial production, such as in automobile engines [10], geothermal energy exploitation [11], natural gas boilers [12], solar thermoelectric cooling systems [13], combined heat and power generation [14], wearable devices [15], energy-autonomous sensors [16], etc.

*Correspondence: yangbo_ac@outlook.com

[1] Faculty of Electric Power Engineering, Kunming University of Science and Technology, Kunming 650500, China
Full list of author information is available at the end of the article

However, the low energy conversion efficiency of TEG systems given unpredictable and ineluctable heterogeneous temperature distribution (HgTD) is the main obstacle that limits its larger scale and wider range of application [17]. To solve this issue, efficient thermoelectric materials and maximum power point tracking (MPPT) technology are considered as two promising solutions [18]. Unfortunately, the former is hard for large-scale applications because of its high cost and long research process [19].

In contrast, MPPT is a more feasible and practical solution. Thus far, a large variety of MPPT approaches have been exploited and employed to capture the global maximum power point (GMPP) of TEG systems under HgTD. Perturb and observe (P&O) [20] and incremental conductance (INC) [21] are two of the most commonly used MPPT strategies because of their simple operational mechanisms. Nevertheless, their performance tends to degrade when multiple local maximum power points (MLMPPs) [22] appear caused by HgTD. Thus, a series of meta-heuristic algorithm (MhAs)-based methods have been proposed to find the GMPP based on their superior global searching ability, e.g., the fast atom search optimizer (FASO) [4], interacted collective intelligence (ICI) [17], adaptive compass search [23], equilibrium optimizer (EO) [22], arithmetic optimization algorithm (AOA) [24], etc. In addition, a novel adaptive rapid neural optimization approach is designed in [25] to realize an available approximation of duty cycle and output power curves for centralized TEG systems through a generalized regression neural network. This significantly reduces power oscillations and energy losses.

It is noteworthy that the aforementioned MPPT methods are all accomplished by controlling the centralized TEG converter to match the impedances of the source and load [26]. This cannot improve the potential GMPP of TEG systems. To fundamentally address this issue, TEG system reconfiguration can be an alternative and effective tool. It is inspired by photovoltaic (PV) system reconfiguration in partial shade conditions (PSC). Specifically, reconfiguration strategies for TEG systems can be divided into two types that are similar to PV system reconfiguration [27], i.e., static and dynamic. Static reconfiguration disperses the temperature difference area by changing the physical position of TEG modules rather than changing electrical connection, while dynamic reconfiguration is capable of dynamically altering the electrical interconnection through switching matrices against various temperature variations. This method generally possesses higher flexibility and lower complexity.

To alleviate adverse effects (e.g., module mismatch, difficulty in tracking the maximum power point, extreme power loss, hot spots, etc. [28]) of partial shading caused by meteorological or geographic factors on PV systems, numerous intensive studies have been done to develop sophisticated technologies on the reconfiguration of PV systems. For instance, a dragonfly algorithm (DA)-based reconfiguration technique for PV systems is proposed in [29]. This is capable of achieving up to 22% output power improvement over conventional methods (e.g., electrical reconfiguration, Sudoku, etc.) under (3×3) and (9×9) arrays. Distinct from MhAs-based techniques, reconfiguration mechanisms enlightened by the magic square puzzle are conceived in [30, 31] to substantially reduce mismatch loss and enhance the GMPP of PV systems. These can offer an appropriate shade dispersion via relocation of PV modules. In addition, reference [32] applies reinforcement learning to the optimal reconfiguration of PV systems under PSC to provide frequency support for the power system.

However, there are not many current studies on the TEG system reconfiguration. In [10], a dynamic reconfiguration algorithm is proposed for a TEG array installed on vehicle radiators, one which can change interconnections (series or parallel) of TEG modules. Nevertheless, it assumes that the temperature difference between the TEG modules connected in parallel in the same row is similar, which is not always guaranteed in large-scale TEG systems. Reference [33] achieves TEG array reconfiguration via adjusting switches with wireless sensors. This is suitable for occasions where wiring is inconvenient.

Although using electrical switchgear is feasible, how to obtain an appropriate switch adjustment scheme is complicated and challenging since dynamic reconfiguration of TEG systems is a nonlinear, discrete, and constrained optimization problem. Furthermore, traditional approaches, e.g., branch and bound as well as enumeration methods, face the risk of combination explosion with increasing dimensionality. Therefore, traditional methods are normally not applicable to the reconfiguration of large-scale TEG systems. To address the above limitations, a novel adaptive coordinated seeker (ACS) is presented here for dynamic reconfiguration of TEG systems under different HgTDs.

The major contributions of this paper can be summarized as follows:

- Dynamic reconfiguration of TEG systems under HgTDs is developed based on MhAs, for the first time.
- ACS is first designed to coordinate the local searching capability of a tabu search (TS) and the global searching capability of a pelican optimization algorithm (POA). This can efficiently overcome drawbacks of traditional MhAs that are highly randomized and heavily dependent on certain parameters.

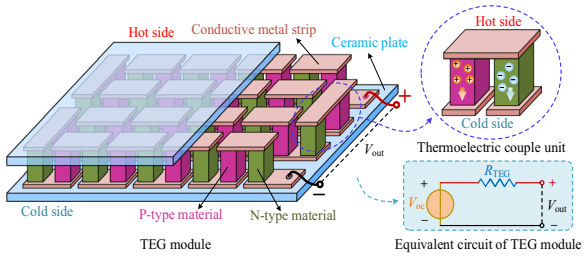

Fig. 1 Schematic of TEG and equivalent circuit of TEG module

- An equivalent re-optimization strategy (EROS) for reconfiguration solutions is developed to reduce unnecessary switching actions.
- The practical and specific performance of an ACS is comprehensively evaluated under two typical scenarios, i.e., symmetrical and asymmetrical, via comparison with seven typical MhAs, i.e., artificial bee colony (ABC) algorithm, ant colony optimization (ACO), genetic algorithm (GA), particle swarm optimization (PSO), simulated annealing (SA) algorithm, TS, and POA.

The rest of this paper is structured as follows: TEG system modeling under HgTD is established in Sect. 2, while Sect. 3 introduces the optimization framework of the ACS. In Sect. 4, the execution process of TEG system reconfiguration and EROS are provided, respectively. Case studies, statistical analysis, and hardware-in-the-loop experiments are carried out in Sect. 5. Finally, main findings and conclusions are drawn in Sect. 6.

2 TEG system modelling

2.1 TEG module modelling

As illustrated in Fig. 1, a TEG module consists of two main components packaged together, i.e., two ceramic plates located on the cold and hot sides, respectively, while multiple thermoelectric couple units are connected in series with conductive metal strips between them. The thermoelectric couple unit is a fundamental and crucial element for a TEG module.

In general, the equivalent circuit of a TEG module is modeled as a voltage source V_{oc} connected with a series resistance R_{TEG} [4]. Here, the open-circuit voltage V_{oc} (V) is directly determined by the temperature difference between the two ceramic plates as [34]:

$$V_{oc} = n_{np} \cdot \alpha_{sb} \cdot \Delta T = n_{np} \cdot \alpha_{sb}(T_{hs} - T_{cs}) \tag{1}$$

where $n_{np}=488$ is the number of thermoelectric units, α_{sb} is the Seeback coefficient (V/K), T_{hs} (K) and T_{cs} (K) represent the temperature of the hot and cold sides, respectively.

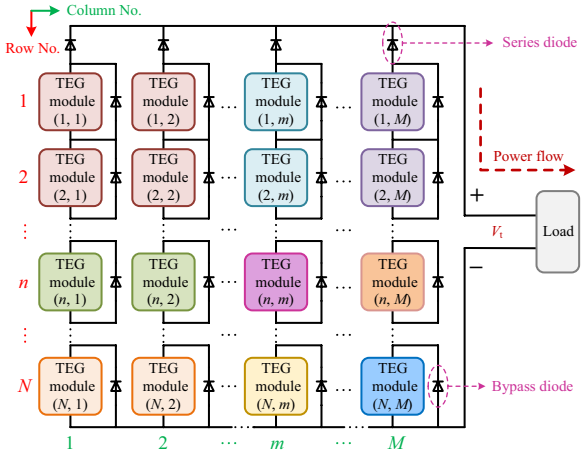

Fig. 2 Configuration of ($N \times M$) TEG system with SP

The relationship between α_{sb} and Thomson coefficient τ (V/K) is given by [22]:

$$\tau = T_{av} \cdot \mathrm{d}\alpha_{sb}/\mathrm{d}T_{av} \tag{2}$$

where T_{av} (K) is the average value of T_{hs} and T_{cs}.

For practical materials, τ is not zero. Thus, α_{sb} can be deduced from (2) as [4]:

$$\alpha_{sb}(T_{av}) = \alpha_{sb0} + \alpha_{sb1} \ln(T_{av}/T_0) \tag{3}$$

where $\alpha_{sb0}=210$ μV/K and $\alpha_{sb1}=120$ μV/K. These are the constant portion and variation rate of α_{sb}, respectively [17, 21, 35]. $T_0=300$ K denotes the temperature reference.

In addition, R_{TEG} is affected by the operational temperature of the TEG module [36]. This can be described as:

$$R_{TEG}(T_{av}) = -2.597 + 0.014T_{av} \tag{4}$$

2.2 TEG system modelling under HgTD

In general, multiple TEG modules are interconnected in an SP electrical connection to obtain the expected voltage level and power density. As shown in Fig. 2, the series diodes are used to avoid circulating current between different strings (columns) within the TEG system when the total voltages of different strings mismatch, while the bypass diodes guarantee that the string with damaged TEG modules still operates normally.

According to the equivalent circuit of a single TEG module illustrated in Fig. 1, the total voltage $V_{oc,m}$ and total internal resistance R_m at the mth string can be expressed as:

$$V_{\mathrm{oc},m} = \sum_{n=1}^{N} (\beta_{n,m} \cdot V_{\mathrm{oc},n,m}) \tag{5}$$

$$R_m = \sum_{n=1}^{N} (\beta_{n,m} \cdot R_{\mathrm{TEG},n,m}) \tag{6}$$

where N is the number of rows in the TEG system, $\beta_{n,m}$ stands for the state of the bypass diode in the nth row and the mth column. This is either 0 (forward conduction) or 1 (reverse cutoff). $V_{\mathrm{oc},n,m}$ and $R_{\mathrm{TEG},n,m}$ represent the open-circuit voltage and internal resistance of the TEG module in the nth row and the mth column, respectively.

Therefore, the mth string is equalized to a voltage resource $V_{\mathrm{oc},m}$ in series with an internal resistance R_m. Based on the Thevenin theorem, the total current I_{total} and total resistance R_{total} of the TEG system can be obtained by:

$$I_{\mathrm{total}} = \sum_{m=1}^{M} (\gamma_m \cdot V_{\mathrm{oc},m}/R_m) \tag{7}$$

$$R_{\mathrm{total}} = 1 \Big/ \sum_{m=1}^{M} (\gamma_m/R_m) \tag{8}$$

$$\gamma_m = \begin{cases} 1, \text{ if } V_{\mathrm{oc},m} > V_{\mathrm{t}} \\ 0, \text{ otherwise} \end{cases} \tag{9}$$

where M is the number of columns in the TEG system, γ_m represents the state of the mth series diode, which is determined by the terminal voltage V_{t} of the TEG system and $V_{\mathrm{oc},m}$.

A voltage vector $[V_0, V_1, V_2, \ldots, V_k, \ldots, V_K]$ $(1 \le K \le M)$ is acquired by sorting the unique values of $[V_0, V_{\mathrm{oc},1}, V_{\mathrm{oc},2}, \ldots, V_{\mathrm{oc},m}, \ldots, V_{\mathrm{oc},M}]$ in ascending order, while $V_0 = 0$ V. According to the maximum power transfer theorem [37], the maximum output power $P_{\mathrm{max},k}$ $(1 \le k \le K)$ can be written when V_{t} falls into the interval of $(V_{k-1}, V_k]$, as:

$$P_{\mathrm{max},k} = (0.5 I_{\mathrm{total}})^2 R_{\mathrm{total}} \tag{10}$$

$$P_{\mathrm{GMPP}} = \max(P_{\mathrm{max},1}, P_{\mathrm{max},2}, \ldots, P_{\mathrm{max},k}, \ldots, P_{\mathrm{max},K}) \tag{11}$$

where K stands for the conductive number of TEG strings.

Hence, the potential GMPP of a TEG system under HgTD can be calculated by Eq. (11) and approached by the aforementioned MPPT techniques.

3 Design of adaptive coordinated seeker

3.1 Tabu search

The TS [38, 39] developed by F. Glover is a widely applied and representative algorithm in combinatorial optimization. It has powerful local searching capability. Its fundamental principle is demonstrated in Table 1, in which neighbourhood structure is defined as the interchange of any two TEG modules within the same row of the TEG system.

3.2 Pelican optimization algorithm (POA)

The swarm-based POA mimics the hunting process of the pelican [40], and has the merits of simple structure and easy implementation. POA contains two principal phases, i.e., moving towards prey and winging on the water surface, as described by (12) and (13), respectively. It should be noted that results are discretized using integer coding with an ascending rule [41], which makes POA applicable to the dynamic reconfiguration of TEG systems.

$$x_i(it+1) = \begin{cases} x_i(it) + r_1 \cdot (x_{\mathrm{p}} - I \cdot x_i(it)), & \text{if } F_{\mathrm{p}} > F_i \\ x_i(it) + r_1 \cdot (x_i(it) - x_{\mathrm{p}}), & \text{otherwise} \end{cases} \tag{12}$$

$$x_i(it+1) = x_i(it) + 0.2(1 - it/It) \cdot (2r_2 - 1) \cdot x_i(it) \tag{13}$$

where $x_i(it)$ and $x_i(it+1)$ indicate the status of the ith pelican in the itth and $(it+1)$th iteration, respectively. x_{p} represents a randomly selected prey from remaining

Table 1 The basic framework of single execution process for TS

Algorithm #1: Single execution process of TS

Input: Neighbourhood structure, neighbourhood size *NS*, tabu table *TT*, length *TL* of *TT*, and feasible solution $x(it)$ and best solution x^* from the itth iteration.

Output: x^*, $x(it+1)$, and *TT*.

1: Generate *NS* candidates for x according to neighbourhood structure;
2: Calculate objective function values of *NS* candidates;
3: Select the best candidate x_{b} from *NS* candidates based on their objective function values;
4: **IF** x_{b} outperforms x^*
5: $x(it+1) \leftarrow x_{\mathrm{b}}$;
6: $x^* \leftarrow x_{\mathrm{b}}$;
7: **ELSE**
8: Obtain best candidate x_{nb} among non-tabu candidates via their objective function values;
9: $x(it+1) \leftarrow x_{\mathrm{nb}}$;
10: **END IF**
11: Update *TT*;
12: Return x^*, $x(it)$, and *TT*;

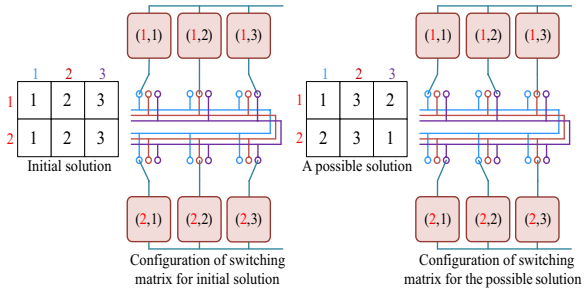

Fig. 3 Coding for solution (2 × 3) and its configuration of the switching matrix

pelicans, while r_1 and r_2 are both random values distributed in the interval of [0, 1]. *It* stands for the maximum iteration, while F_p and F_i are objective function values of x_p and $x_i(it)$, respectively.

3.3 Adaptive coordinated seeker

Based on the idea of parallelism, the entire population is divided equally and randomly into two subpopulations to execute different operations separately. All individuals for the first subpopulation perform algorithm #1 in Table 1. The neighbourhood size of each individual is adaptively adjusted according to its objective function value, as indicated in (14). Therefore, the drawback of traditional TS with heavy dependence on starting solution and search efficiency can be effectively lessened.

$$NS_j = \begin{cases} NS_0 + NoSP - 1, & \text{for best individual} \\ NS_0 - 1, & \text{otherwise} \end{cases} \quad (14)$$

where NS_j is the neighbourhood size of the *j*th individual, with $j = 1, 2, \ldots, NoSP$. NS_0 is the initial neighbourhood size of each individual, and *NoSP* stands for the individual number per subpopulation, which is equal to *NP*/2.

For the second subpopulation, two different operations can be selected with the same probability, i.e., the discretized POA and TS without tabu. In addition, similar to the first subpopulation, the concept of neighbourhood search with adaptive adjustment is used for each individual of the second subpopulation.

To ensure communication between the two subpopulations, the top 20% of the row vectors with the largest difference between the optimal individuals of the two subpopulations are swapped in order after certain iterations (0.04*It*). For instance, the differences between the rows for the two solutions in Fig. 3 are 2/3 and 1, respectively. An effective updating mechanism [40] is adopted during the optimization of ACS to obtain a better solution. The overall ACS implementation procedure for the TEG system dynamic reconfiguration is provided in Fig. 4.

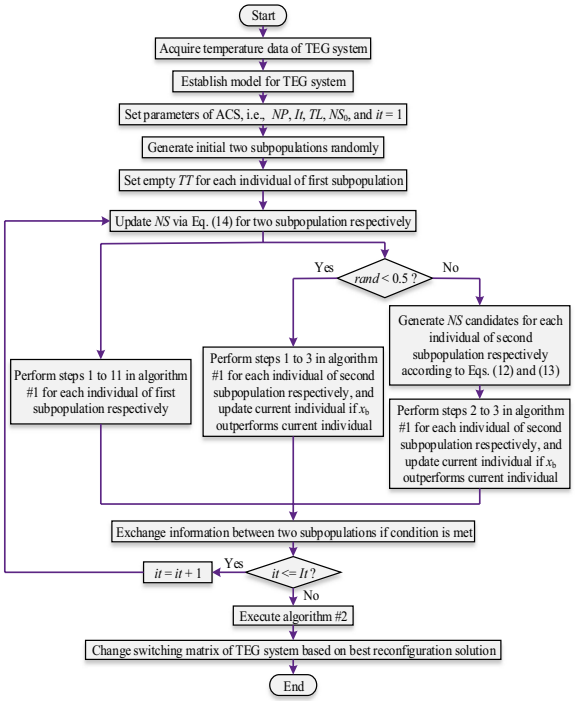

Fig. 4 The overall implementation procedure of dynamic reconfiguration for a TEG system via ACS

As the discretized POA has strong global search ability, it can effectively avoid the problem of premature convergence. In contrast, the mutation mechanism is employed in [42] to improve the PSO for parameter optimization of a transient stability prediction model, which can ensure population diversity. TS is biased to local exploitation,

Table 2 The procedure of EROS for reconfiguration solution

Algorithm #2: EROS

Input: Reconfiguration solution x^* obtained by MhA, and temperature distribution of TEG system.

Output: Equivalently optimized reconfiguration solution ex^*.

$ex^* \leftarrow x^*$;
FOR1 n=1:N
  FOR2 m=1:M
    IF temperature distributions of modules (n, $ex^*(n, m)$) and (n, m) are identical
      $temp \leftarrow ex^*(n, m)$;
      $ex^*(n, m) \leftarrow ex^*(n, ex^*(n, m))$;
      $ex^*(n, ex^*(n, m)) \leftarrow temp$;
    END IF
  END FOR2
END FOR1
Return ex^*;

which can reasonably prevent ACS from blind search. Similarly, reference [43] constructs the memetic algorithm using a binary differential evolution algorithm and TS to extract optimal feature subsets for transient stability assessment of the power system. This can retain valid information to the greatest extent.

4 Dynamic reconfiguration of TEG system via ACS

4.1 Coding and switching matrix

For dynamic reconfiguration, each solution represents one arrangement mode while variables are the column serial number of each module in the TEG system, and the change of module locations is achieved by switching matrices. As shown in Fig. 2, reconfiguration within the same column has no impact for P_{GMPP} as the TEG modules in the same column are connected in series. Therefore, consecutive integer coding from 1 to M (column serial number of modules) is only adopted separately for each row of the TEG system. For instance, the initial solution and a possible solution, and their corresponding configuration of the switching matrices are shown in Fig. 3 for a (2×3) TEG system.

4.2 Objective function and constraints

Dynamic reconfiguration of the TEG system aims to maximize its potential GMPP, while a high-quality solution corresponds to a high potential GMPP. Therefore, the objective function is designed as:

$$x^* = \underset{x^* \in X}{\operatorname{argmax}}\ P_{\mathrm{GMPP}} \tag{15}$$

where X means the feasible solution space and x^* represents the optimal solution.

Moreover, dynamic reconfiguration is performed between different TEG modules in the same row. Thus, a feasible solution x should satisfy the following constraints:

$$\begin{cases} x(n,m) \in \{1,2,...,M\} \\ \bigcup_{m=1}^{M} x(n,m) = \{1,2,...,M\} \end{cases} \tag{16}$$

where $x(n,m)$ is the variable value of the nth row and the mth column in the feasible solution x.

4.3 Equivalent re-optimization of reconfiguration solution

Reconfiguration solutions obtained by various MhAs may not be in an optimal form under the same P_{GMPP} because of the inherent randomness of MhAs and the non-uniqueness of the solution. For example, assuming that the temperature conditions for modules (1,2) and (1,3) in Fig. 3 are identical, the two modules are completely equivalent according to (1) and (4). Thus, the switching states for modules (1,2) and (1,3) of the possible solution can also be consistent with the initial states. However, if the operation is performed directly following the possible solution, unnecessary switching actions will be caused. Therefore equivalent re-optimization for reconfiguration solutions obtained by various MhAs is essential and meaningful based on the temperature distribution of the TEG system. Its detailed procedure is tabulated in Table 2.

4.4 Implementation process of dynamic reconfiguration for TEG system using ACS

Figure 4 explicitly demonstrates the overall implementation procedure of dynamic reconfiguration for the TEG system using ACS. *rand* stands for a random value distributed in the interval of [0, 1]. It is worth noting that the initial arrangement of the TEG system needs to be included in the population during random initialization to ensure an effective optimization. Additionally, a basic precondition for this work is that the operating temperatures of each module in the TEG system can be collected by measuring devices.

5 Case studies

To validate the dynamic reconfiguration performance of ACS for the TEG systems under various HgTDs, two typical scenarios are developed, i.e., symmetrical (15×15) and asymmetrical configuration (20×15). Furthermore, four typical temperature distributions are studied for each configuration, including diagonal, outer, inner, and random [28]. Seven conventional MhAs, e.g., ABC [44], ACO [45], GA [28], PSO [28], SA [41], TS [38, 39], and POA [40], are used for comparison with ACS. For a fair comparison, NP and It are uniformly set as ($NP=30$, $It=500$) and ($NP=30$, $It=1000$) under symmetrical and asymmetrical scenarios, respectively. All algorithms are independently executed 50 times to obtain the statistical results, while all simulations are executed in the MATLAB/Simulink 2019b environment with a personal computer with Intel(R) Core(TM) i5 CPU at 2.9 GHz and 16 GB of RAM, and ode45 (Dormand-Prince) with variable step chosen as the solver.

5.1 Symmetrical configuration

Figures 5 and 6 illustrate the initial and optimal temperature distributions acquired by ACS in a symmetrical TEG system (15×15) under four different scenarios. Boxplots of the maximum output power obtained by eight algorithms under the four different scenarios of the (15×15) TEG system are shown in Fig. 7. This reveals the statistical distribution of the maximum output power for each algorithm in 50 runs. Clearly ACS can obtain the highest average

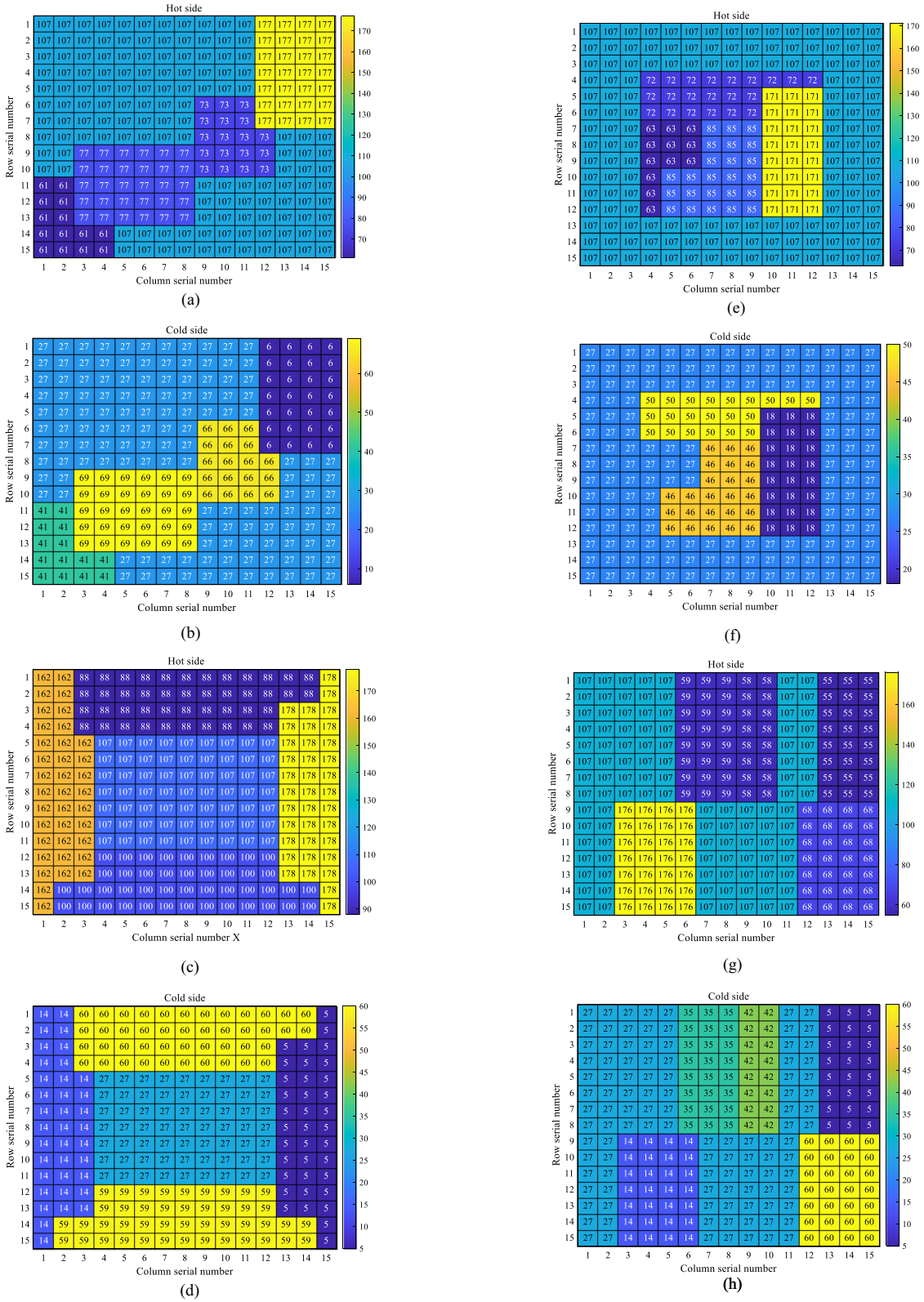

Fig. 5 Initial temperature distribution (°C) of four different scenarios for (15 × 15) TEG system: **a**, **b** diagonal, **c**, **d** outer, **e**, **f** inner, **g**, **h** random

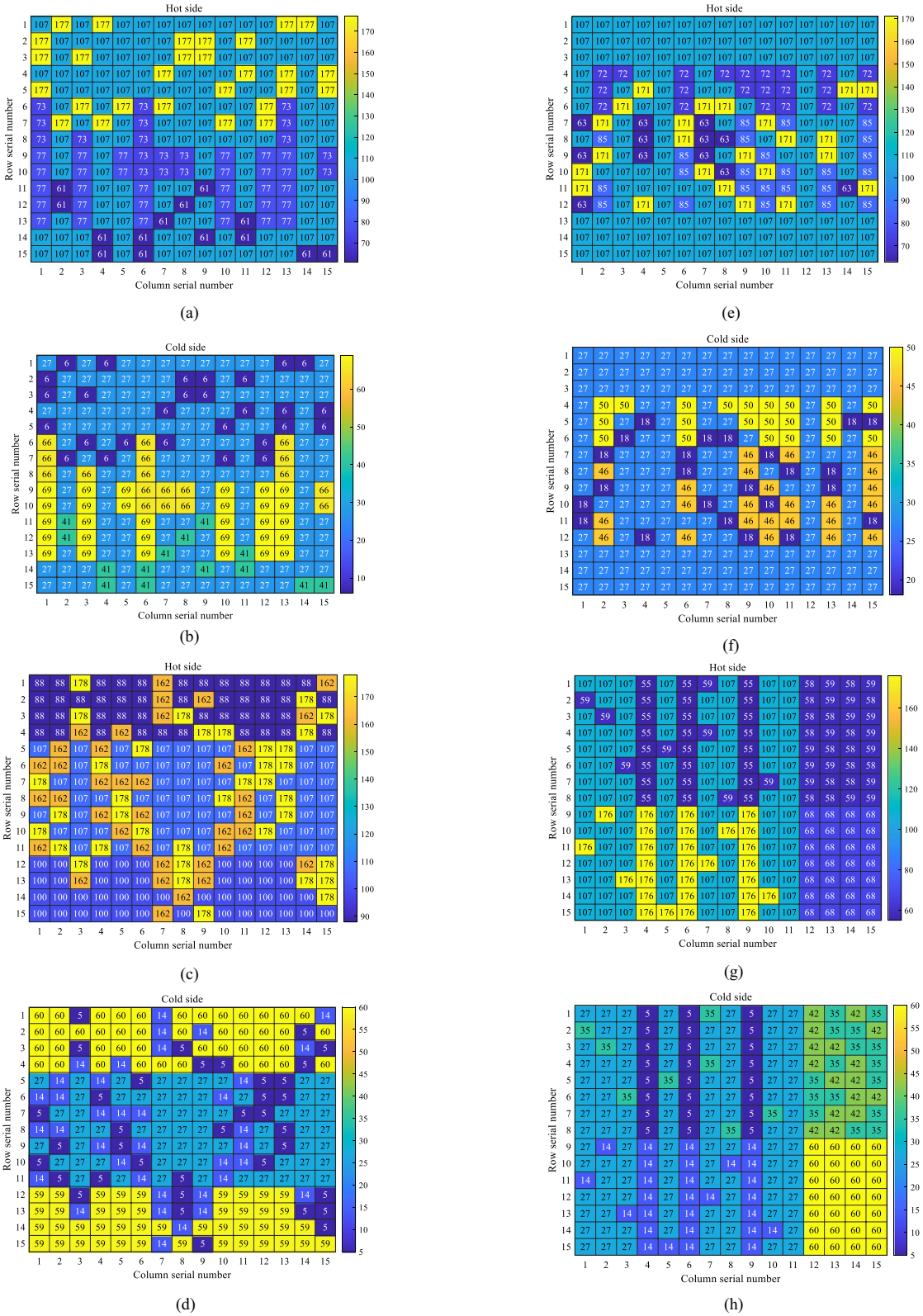

Fig. 6 Temperature distribution (°C) of four different scenarios for (15 × 15) optimized by ACS: **a**, **b** diagonal, **c**, **d** outer, **e**, **f** inner, **g**, **h** random

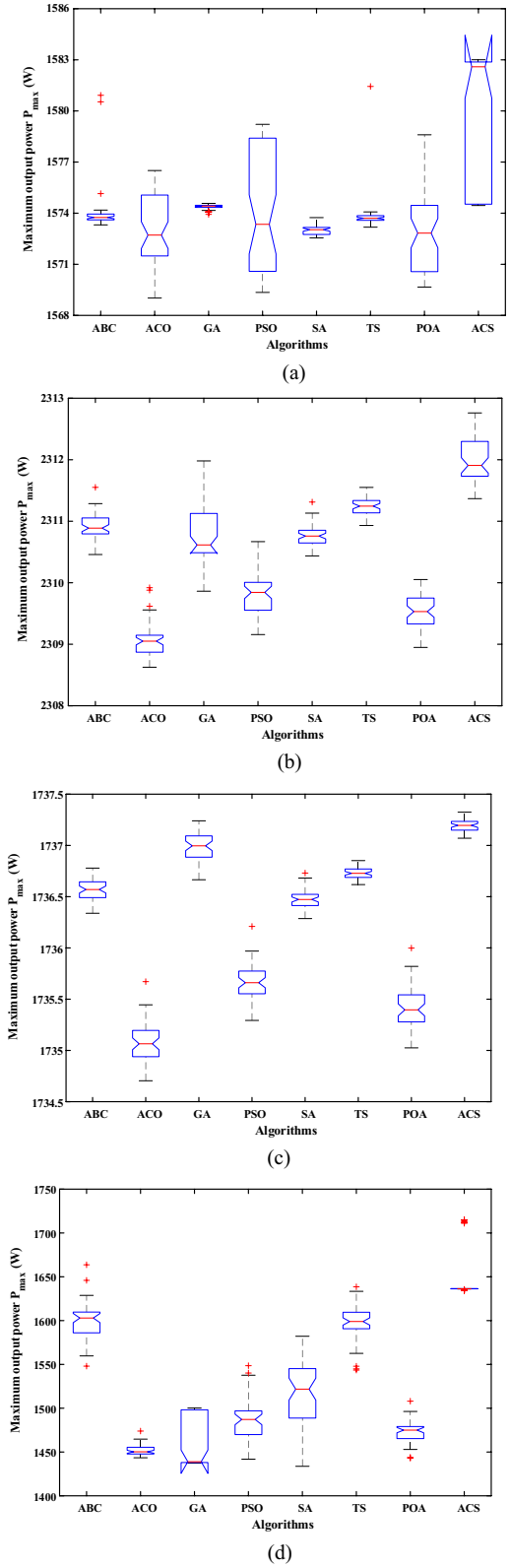

Fig. 7 Boxplots of maximum output power obtained by eight algorithms under four different scenarios of a (15 × 15) TEG system: **a** diagonal, **b** outer, **c** inner, and **d** random

value of the maximum output power of the TEG system. In particular, the distribution range of the maximum output power acquired from ACS is the smallest in the outer, inner, and random conditions. Thus, it can be seen that ACS has superior performance in terms of convergence stability and expectation of the maximum output power.

Figure 8 draws the convergence curves of various algorithms for the four different TEG systems, where ACS can converge within 350 iterations along with optimum output power under the four conditions. As depicted in Fig. 8b, c, although ABC has a faster convergence speed in the early iterations, it falls into a local optimum solution in the late stages, which further proves the superior global searching capability of ACS.

The power-voltage (P–V) and current–voltage (I–V) curves of the TEG systems before and after optimization using ACS are shown in Fig. 9. It can be seen that the potential GMPPs of the TEG systems are notably enhanced by 3.4%, 4.5%, 2.7%, and 22.8% via ACS under diagonal, outer, inner, and random scenarios, respectively. In addition, the total voltage difference between the different strings in the TEG system is significant when the temperature is regionally and intensively distributed as shown in Fig. 5. Hence, MLMPPs phenomena are inevitably induced because of the presence of series diodes [4, 22, 23]. More specifically, the voltage discrepancy among different strings will be decreased on account of uniform temperature distributions in the row direction obtained by ACS as in Fig. 6, and thus MLMPPs phenomena of P–V curves are significantly reduced, as shown in Fig. 9.

5.2 Asymmetrical configuration

To further validate the superiority of ACS under various HgTDs, an asymmetrical TEG configuration (20 × 15) is designed and comprehensively evaluated. The initial and optimized temperature distributions based on ACS are shown in Figs. 10 and 11, respectively. It can be easily seen that temperatures in Fig. 11 are uniformly distributed in the row direction under all tested HgTDs.

As delineated in Fig. 12, the distribution of the output power generated from 50 independent reconfigurations of the (20 × 15) TEG system by ACS is more centralized than others, where the acquired lower and upper bounds of output power are higher.

It is seen in Fig. 13 that faster convergence and higher output power are achieved by ACS. In contrast, other algorithms, particularly ACO, PSO, and POA, tend to suffer from worse reconfiguration solutions with inferior convergence rates. Based on the above analysis and discussion, it is shown that ACS can rapidly provide reconfiguration solutions for TEG systems with high desired output power.

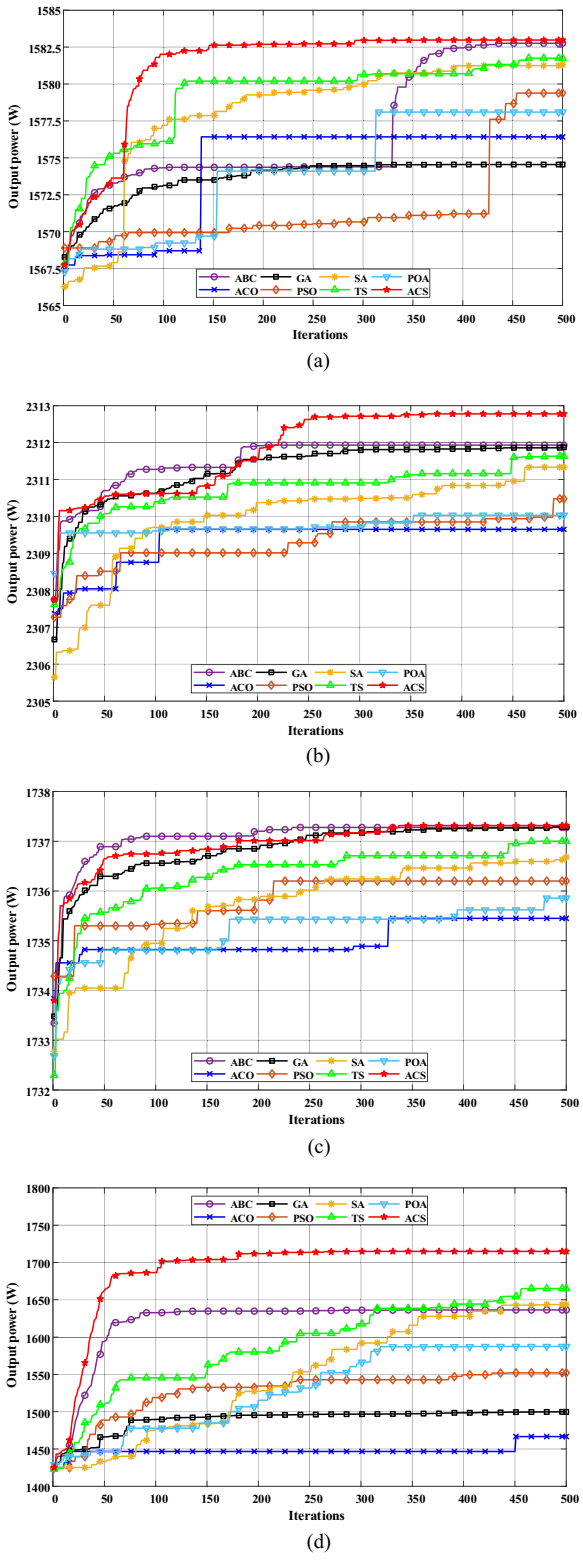

Fig. 8 Convergence curves of eight algorithms under four different scenarios of (15 × 15) TEG system: **a** diagonal, **b** outer, **c** inner, and **d** random

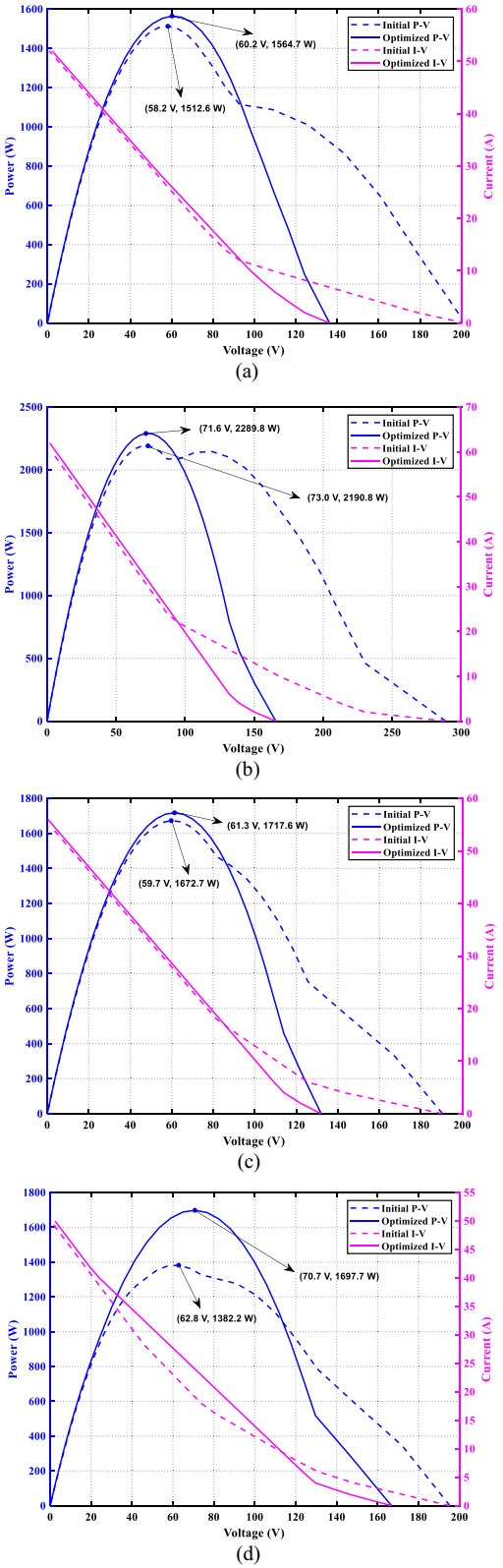

Fig. 9 Output characteristics of (15 × 15) TEG system under four different scenarios before and after being optimized by ACS: **a** diagonal, **b** outer, **c** inner, and **d** random

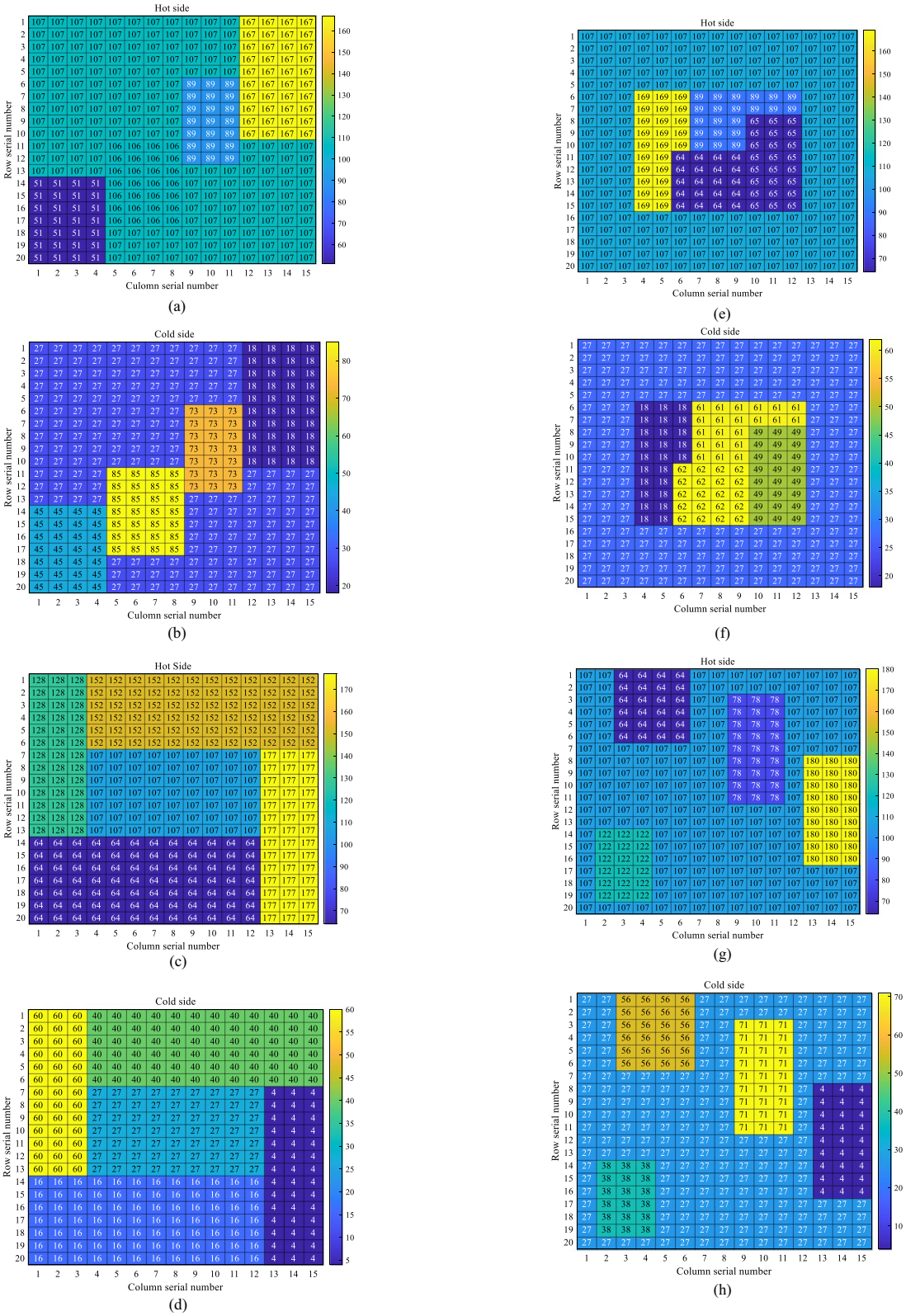

Fig. 10 Initial temperature distribution (°C) of four different scenarios for (20 × 15) TEG system: **a**, **b** diagonal, **c**, **d** outer, **e**, **f** inner, **g**, **h** random

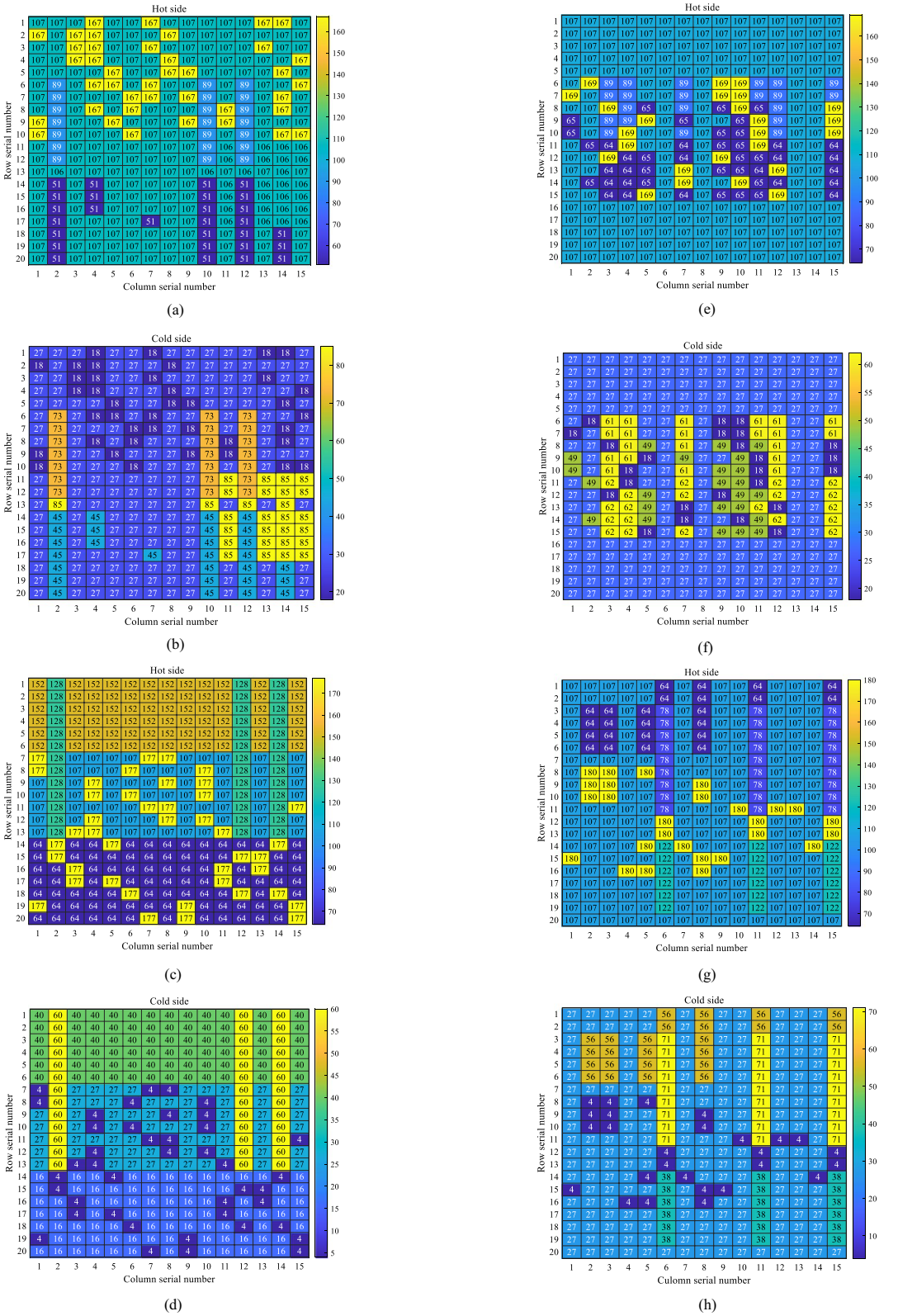

Fig. 11 Temperature distribution (°C) of four different scenarios for (20 × 15) optimized by ACS: **a**, **b** diagonal, **c**, **d** outer, **e**, **f** inner, **g**, **h** random

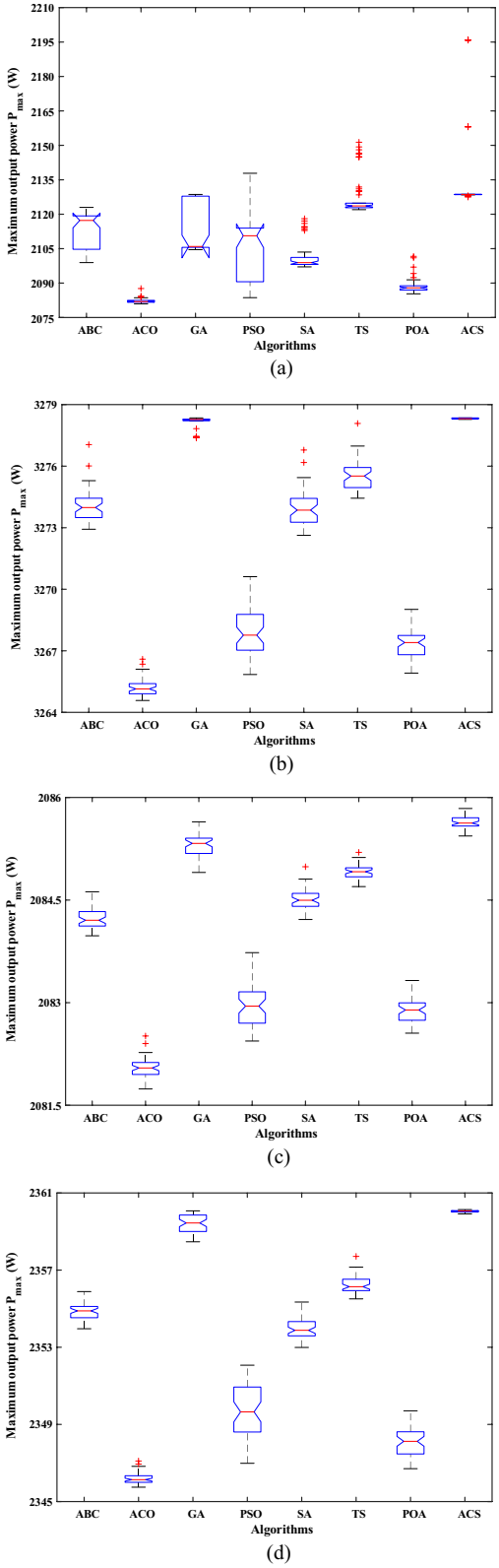

Fig. 12 Convergence curves of eight algorithms under four different scenarios of (20 × 15) TEG system: **a** diagonal, **b** outer, **c** inner, and **d** random

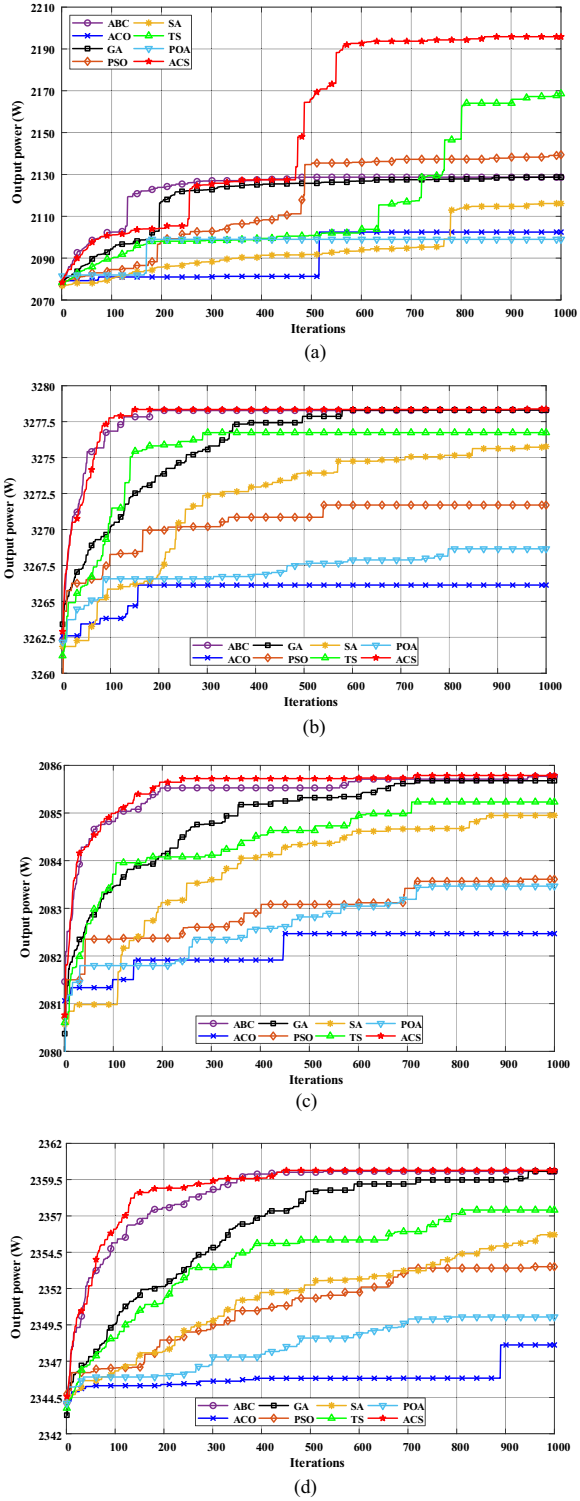

Fig. 13 Convergence curves of eight algorithms under four different scenarios of a (20 × 15) TEG system: **a** diagonal, **b** outer, **c** inner, and **d** random

Figure 14 shows the output characteristics of the TEG system under the four different scenarios. This indicates that potential GMPPs corresponding to the optimal solutions are respectively boosted by 164.0 W, 122.8 W, 34.7 W, and 47.4 W, compared to those of the initial solutions. The output characteristics are also significantly smoothed via ACS, which significantly alleviates the burden and complexity of MPPT.

5.3 Analysis and discussion for statistical results

Tables 3 and 4 provide statistical results obtained by the eight methods in 50 independent runs under the symmetrical and asymmetrical scenarios, respectively, where the optimal results are shown in bold. Although all methods can improve the output power of the TEG systems because of their original arrangements being used as the initial solutions of each method, ACS can harvest the highest output power and maximum average output power under all cases. In particular, in the symmetrical TEG system with random temperature distribution, the maximum output power of ACS is 103.1%, 116.3%, 114.3%, 110.7%, 108.4%, 104.7%, and 113.7% of that of ABC, ACO, GA, PSO, SA, TS, and POA, respectively. In addition, GMPPs of the optimized P–V curves in Fig. 14 are 16.9 W, 23.1 W, 18.7 W, and 19.8 W lower than the best results obtained by ACS in Table 4 under the four scenarios, respectively. This result is mainly caused by the forward conduction losses on the diodes.

As illustrated in Tables 3 and 4, both ACS and TS can obtain reconfiguration solutions with similar maximum output power under two HgTDs (i.e., outer and inner), which indicates that they have similar performance in these scenarios. However, as mentioned above, ACS is superior to TS in terms of convergence speed and stability, as displayed in Figs. 7, 8, 12, and 13. Overall, it is evident that ACS is successfully applied to the dynamic reconfiguration of the TEG systems with high accuracy, fast convergence speed, and excellent stability.

Table 5 tabulates the action module number reduced by EROS for the optimal solution of each algorithm in both symmetrical and asymmetrical scenarios. It is apparent that EROS can noticeably reduce the number of action modules in all cases. Hence, unnecessary switching actions and reconfiguration costs can be considerably reduced.

5.4 RTLAB based hardware-in-the-loop experiments

RTLAB platform-based hardware-in-the-loop experiments are carried out to further validate the hardware implementation feasibility, as shown in Fig. 15, with a sampling frequency of 1 kHz. Figures 16 and 17

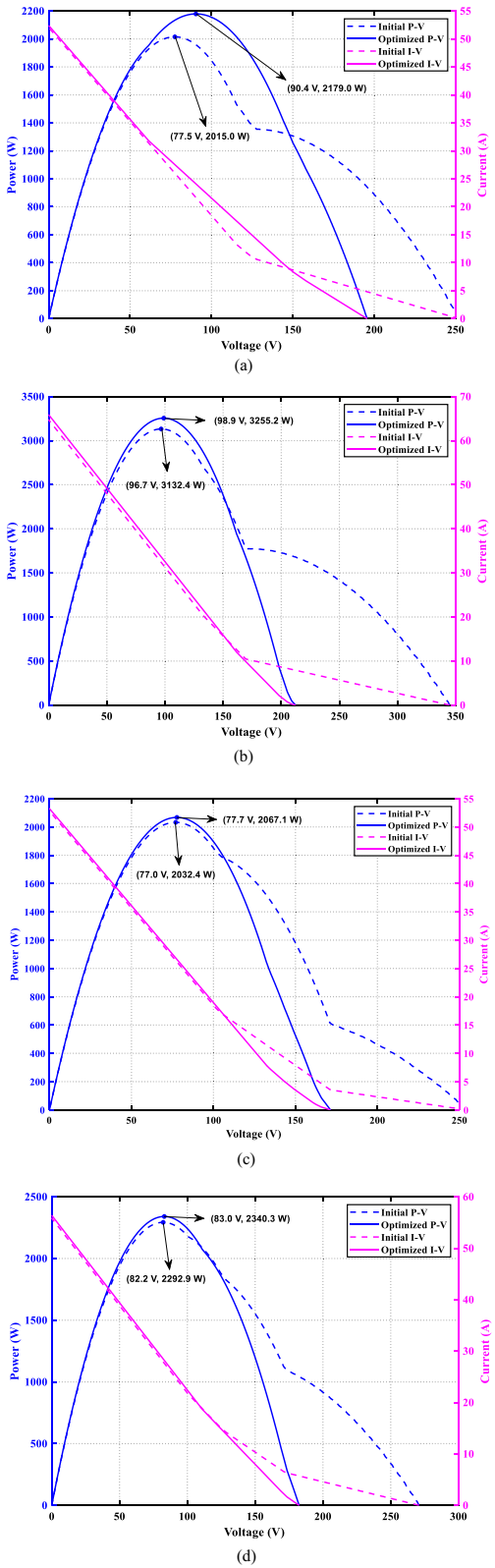

Fig. 14 Output characteristics of (20 × 15) TEG system under four different scenarios before and after being optimized by ACS: **a** diagonal, **b** outer, **c** inner, and **d** random

Table 3 Statistical results obtained by each algorithm under four different scenarios of a (15 × 15) TEG system

Algorithms	Indexes	Scenarios			
		Diagonal	Outer	Inner	Random
Initial solution	Maximum output (W)	1531.1	2213.7	1692.4	1399.1
ABC	Best (W)	1580.9	2311.6	1736.8	1663.7
	Mean (W)	1574.1	2310.9	1736.6	1598.8
ACO	Best (W)	1576.5	2309.9	1735.7	1473.9
	Mean (W)	1572.9	2309.1	1735.1	1451.9
GA	Best (W)	1574.6	2312.0	1737.2	1500.2
	Mean (W)	1574.4	2310.8	1737.0	1458.9
PSO	Best (W)	1579.2	2310.7	1736.2	1548.6
	Mean (W)	1574.3	2309.8	1735.7	1486.7
SA	Best (W)	1573.7	2311.3	1736.7	1582.1
	Mean (W)	1573.0	2310.8	1736.5	1519.5
TS	Best (W)	1581.4	2311.6	1736.9	1638.5
	Mean (W)	1573.9	2311.2	1736.7	1598.0
POA	Best (W)	1578.6	2310.1	1736.0	1508.1
	Mean (W)	1572.9	2309.5	1735.4	1472.7
ACS	Best (W)	**1583.0**	**2312.8**	**1737.3**	**1714.9**
	Mean (W)	**1579.1**	**2312.0**	**1737.2**	**1646.9**

Table 4 Statistical results obtained by each algorithm in four different scenarios of a (20 × 15) TEG system

Algorithms	Indexes	Scenarios			
		Diagonal	Outer	Inner	Random
Initial solution	Maximum output (W)	2033.3	3155.2	2051.0	2312.6
ABC	Best (W)	2123.0	3277.0	2084.6	2355.9
	Mean (W)	2113.6	3274.1	2084.2	2354.9
ACO	Best (W)	2087.6	3266.6	2082.5	2347.1
	Mean (W)	2082.2	3265.2	2082.0	2346.2
GA	Best (W)	2128.6	3278.3	2085.6	2360.1
	Mean (W)	2115.3	3278.1	2085.3	2359.4
PSO	Best (W)	2137.8	3270.6	2083.7	2352.1
	Mean (W)	2106.4	3268.0	2083.0	2349.7
SA	Best (W)	2118.1	3276.8	2085.0	2355.3
	Mean (W)	2101.3	3274.0	2084.5	2354.0
TS	Best (W)	2151.4	3278.1	2085.2	2357.7
	Mean (W)	2127.4	3275.5	2084.9	2356.2
POA	Best (W)	2101.6	3269.0	2083.3	2349.7
	Mean (W)	2088.7	3267.4	2082.9	2348.1
ACS	Best (W)	**2195.9**	**3278.3**	**2085.8**	**2360.1**
	Mean (W)	**2138.4**	**3278.3**	**2085.6**	**2360.1**

demonstrate the output characteristics of each TEG system under various HgTDs optimized by ACS. It can be seen from Figs. 16 and 17 that the responses of the simulation and experiment acquired by the two configurations under several HgTDs are largely similar.

6 Conclusions

In this work, a novel ACS is designed to realize an effective and efficient dynamic reconfiguration of two different TEG systems, i.e., symmetrical and asymmetrical under various HgTDs. The main conclusions are:

Table 5 Action modules reduced by EROS for optimal solution of each algorithm in symmetrical and asymmetrical

TEG systems	Algorithms	Scenarios			
		Diagonal	Outer	Inner	Random
Symmetrical (15 × 15)	ABC	89	102	122	35
	ACO	96	102	115	59
	GA	103	102	120	53
	PSO	104	110	116	57
	SA	103	105	126	85
	TS	97	104	120	88
	POA	100	104	111	62
	ACS	95	98	114	19
Asymmetrical (20 × 15)	ABC	127	42	187	164
	ACO	126	162	167	142
	GA	114	168	169	142
	PSO	132	180	180	145
	SA	129	183	192	149
	TS	120	145	164	138
	POA	118	161	179	153
	ACS	112	171	186	153

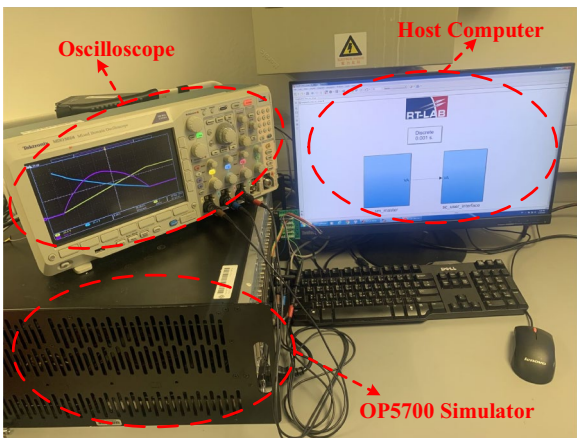

Fig. 15 Hardware-in-the-loop experiment using RTLAB platform

1. An MhA-based dynamic reconfiguration strategy for large-scale TEG systems is presented and accomplished for the first time. It aims to re-use waste heat generated in daily life and industrial production.
2. Compared with traditional MhAs, ACS is able to execute a reasonable equilibrium between global exploration and local exploitation via simultaneous execution of TS and discretized POA. Therefore, ACS can accurately and rapidly converge to optimal reconfiguration solutions for TEG systems under various HgTDs with a higher probability.

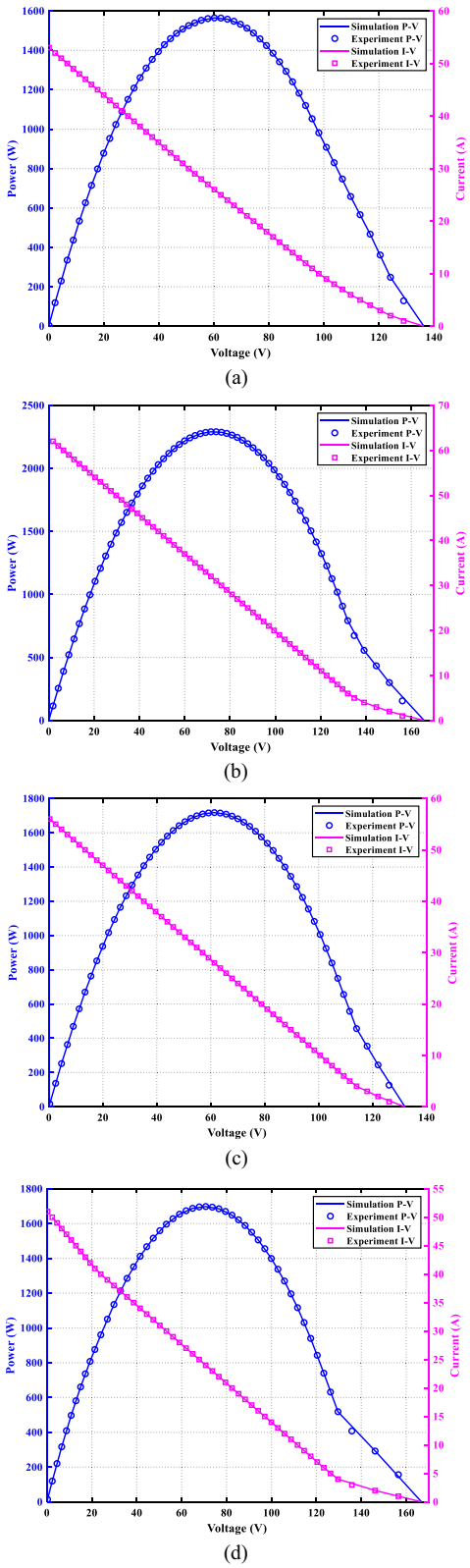

Fig. 16 Output characteristics of (15 × 15) TEG system for simulation and experiment under various HgTDs optimized by ACS: **a** diagonal, **b** outer, **c** inner, and **d** random

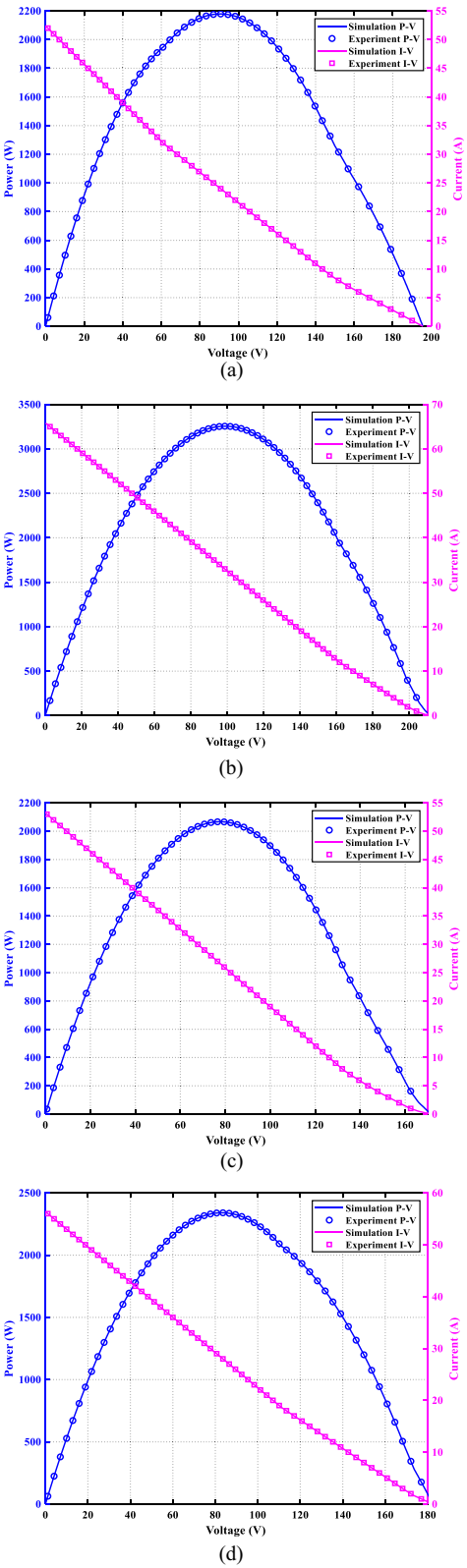

Fig. 17 Output characteristics of (20 × 15) TEG system for simulation and experiment under various HgTDs optimized by ACS: **a** diagonal, **b** outer, **c** inner, and **d** random

3. Comprehensive case studies verify that ACS has a better performance in dynamic reconfiguration than other MhAs. In particular, the maximum output power of ACS is 103.1%, 116.3%, 114.3%, 110.7%, 108.4%, 104.7%, and 113.7% of that of ABC, ACO, GA, PSO, SA, TS, and POA under symmetrical scenario with random temperature distribution, respectively. The expected output power is enhanced by 34.6 W-247.8 W via ACS compared with that of initial solutions under eight HgTDs, which further validates that ACS can significantly improve the potential GMPP of TEG systems.
4. Statistical results show that EROS can significantly reduce the number of action modules required under various cases. This can boost the practicability and economy of TEG systems with low generation efficiency.

However, it is necessary to reasonably set the number of individuals and iterations of ACS according to the scale of the TEG system in practical application in order to obtain an acceptable computational cost. The completion of the dynamic reconfiguration of the TEG system relies highly on accurate and reliable temperature measurement equipment, which increases the cost. Therefore, the deployment of the thermometer and operator of ACS can be further optimized, while ACS can be extended to the reconfiguration of PV and PV-TEG systems in future studies.

List of symbols

α_{sb}: Seeback coefficient (V/K); α_{sb0}: Constant portion of α_{sb} (V/K); α_{sb1}: Variation rate of α_{sb} (V/K); $\beta_{n,m}$: State of bypass diode in the nth row and the mth column; γ_m: State of the mth series diode; τ: Thomson coefficient (V/K); it: Current iterations of pelican optimization algorithm; It: Maximum iterations of pelican optimization algorithm; I_{total}: Total current of TEG system (A); M: Number of columns in TEG system; N: Number of rows in TEG system; NP: Total number of individuals of each algorithm; n_{np}: Number of thermoelectric units; P_{GMPP}: Global maximum output power of TEG system (W); R_{TEG}: Internal resistance of TEG system (Ω); $R_{TEG,n,m}$: Internal resistance of TEG module in the nth row and the mth column (Ω); R_m: Total internal resistance of the mth module (Ω); R_{total}: Total resistance of TEG system (Ω); T_{hs}: Temperature of hot side (K); T_{cs}: Temperature of cold side (K); T_{av}: Average value of T_{hs} and T_{cs} (K); T_0: Temperature reference (K); V_{oc}: Open-circuit voltage of TEG module (V); $V_{oc,m}$: Total open-circuit voltage of the mth module (V); $V_{oc,n,m}$: Open-circuit voltage of TEG module in the nth row and the mth column (V); V_t: Terminal voltage of TEG system (V); X: Feasible solution space; x: A solution in X; x_i: Status of the ith pelican; x^*: Optimal solution.

Abbreviations

ACS: Adaptive coordinated seeker; AOA: Arithmetic optimization algorithm; ABC: Artificial bee colony; ACO: Ant colony optimization; DA: Dragonfly algorithm; EO: Equilibrium optimizer; EROS: Equivalent re-optimization strategy; FASO: Fast atom search optimizer; GMPP: Global maximum power point; GA: Genetic algorithm; HgTD: Heterogeneous temperature distribution; INC: Incremental conductance; ICI: Interacted collective intelligence; MPPT: Maximum power point tracking; MLMPPs: Multiple local maximum power points; MhAs: Meta-heuristic algorithms; P&O: Perturb and observe; PV: Photovoltaic; PSC: Partial shading conditions; POA: Pelican optimization algorithm; PSO: Particle swarm optimization; SP: Series–parallel; SA: Simulated annealing; TS: Tabu search; TEG: Thermoelectric generation.

Acknowledgements
The authors appreciatively acknowledge the support of by National Natural Science Foundation of China (61963020).

Author contributions
YC: Conceptualization, methodology, writing, and software; BY: Writing-review and editing; ZG: Investigation, and visualization; JW: Supervision, writing-review, and editing; MZ: Writing-reviewing, editing, and methodology; ZL: Experiment and software; TY: Supervision, project administration, resources, and data curation. All authors read and approved the final manuscript.

Authors' Information
Yijun Chen (1996–), male, Master Degree Candidate, Major in the renewable energy optimization and control.
Bo Yang (1988–), male, PHD and Professor, Major in the intelligent optimization and control of renewable energy and energy storage system.
Zhengxun Guo (1998–), male, Master Degree Candidate, Major in the renewable energy optimization and control.
Jingbo Wang (1996–), male, Master Degree, Major in the optimization operation of photovoltaic system.
Mengmeng Zhu (1986–), male, PHD Candidate and Engineer, Major in the voltage and current transformers.
Zilin Li (1988–), male, PHD, Major in the electric power electronic power system stability and operation.
Tao Yu (1974–), PHD and Professor, Major in the nonlinear control theory, optimization for complex power systems, and machine learning.

Funding
National Natural Science Foundation of China (61963020).

Availability of data and materials
The datasets used or analyzed during the current study are available from the corresponding author on reasonable request.

Declarations

Competing interests
The authors declare that they have no known competing financial interests or personal relationships that could have appeared to influence the work reported in this paper.

Author details
[1]Faculty of Electric Power Engineering, Kunming University of Science and Technology, Kunming 650500, China. [2]Electric Power Research Institute of Yunnan Power Grid Co., Ltd, Kunming 650217, China. [3]Department of Electrical Engineering, Hong Kong Polytechnic University, Kowloon 999077, Hong Kong SAR, China. [4]College of Electric Power, South China University of Technology, Guangzhou 510640, China.

Received: 17 June 2022 Accepted: 19 September 2022
Published online: 10 October 2022

References

1. Papież, M., Śmiech, S., & Frodyma, K. (2019). Effects of renewable energy sector development on electricity consumption-Growth nexus in the European Union. *Renewable and Sustainable Energy Reviews, 113*, 109276.
2. Cheng, S., Wang, Y.-Q., Liao, W.-L., Zuo, X.-W., & Dai, J. (2022). Bi-level multi-objective optimization of a new energy microgrid with electric vehicles. *Power System Protection and Control, 50*(12), 63–71. https://doi.org/10.19783/j.cnki.pspc.211149
3. Wang, Z., Li, L.-L., Li, Z.-H., Cheng, Z.-Y., Yao, W.-F., & Liu, R.-S. (2021). The evolution characteristics of power grid frequency probability distribution. *Power System Protection and Control, 49*(20), 65–73. https://doi.org/10.19783/j.cnki.pspc.201654
4. Yang, B., Zhang, M.-T., Zhang, X.-S., Wang, J.-B., Shu, H.-C., Li, S.-N., He, T.-Y., Yang, L., & Yu, T. (2020). Fast atom search optimization based MPPT design of centralized thermoelectric generation system under heterogeneous temperature difference. *Journal of Cleaner Production, 248*, 119301.
5. Guo, Y.-F., Gao, H.-L., & Wu, Q.-W. (2017). A combined reliability model of VSC-HVDC connected offshore wind farms considering wind speed correlation. *IEEE Transactions on Sustainable Energy, 8*(4), 1637–1646.
6. Li, G.-Q., Shittu, S., Diallo, T. M. O., Yu, M., Zhao, X.-D., & Ji, J. (2018). A review of solar photovoltaic-thermoelectric hybrid system for electricity generation. *Energy, 158*, 41–58.
7. Fu, X. (2022). Statistical machine learning model for capacitor planning considering uncertainties in photovoltaic power. *Protection and Control of Modern Power Systems, 7*, 5.
8. Abd El-Kareem, A. H., Abd Elhameed, M., & Elkholy, M. M. (2021). Effective damping of local low frequency oscillations in power systems integrated with bulk PV generation. *Protection and Control of Modern Power Systems, 6*, 41.
9. Tohidi, F., Holagh, S. G., & Chitsaz, A. (2022). Thermoelectric generators: A comprehensive review of characteristics and applications. *Applied Thermal Engineering, 201*, 117793.
10. Kim, J., Baek, D., Ding, C.-W., Lin, S., Shin, D., Lin, X., Wang, Y.-Z., Hoo-Cho, Y., Park, S. H., & Chang, N. (2018). Dynamic reconfiguration of thermoelectric generators for vehicle radiators energy harvesting under location-dependent temperature variations. *IEEE Transactions on Very Large Scale Integration (VLSI) Systems, 26*(7), 1241–1253.
11. Catalan, L., Aranguren, P., Araiz, M., Perez, G., & Astrain, D. (2019). New opportunities for electricity generation in shallow hot dry rock fields: A study of thermoelectric generators with different heat exchangers. *Energy Conversion and Management, 200*, 112061.
12. Zhao, Y.-L., Wang, S.-X., Ge, M.-H., Li, Y.-Z., & Liang, Z.-J. (2017). Analysis of thermoelectric generation characteristics of flue gas waste heat from natural gas boiler. *Energy Conversion and Management, 148*, 820–829.
13. Shen, Z.-H., Ni, H., Ding, C., Sui, G.-R., Jia, H.-Z., Gao, X.-M., & Wang, N. (2021). Improving the energy-conversion efficiency of a PV-TE system with an intelligent power-track switching technique and efficient thermal-management scheme. *IEEE Transactions on Components, Packaging and Manufacturing Technology, 11*(6), 963–973.
14. Montecucco, A., Siviter, J., & Knox, A. R. (2017). Combined heat and power system for stoves with thermoelectric generators. *Applied Energy, 185*(Part 2), 1336–1342.
15. Shiotsu, Y., Seino, T., Kondo, T., & Sugahara, S. (2020). Modeling and design of thin-film pi-type micro thermoelectric generator using vacuum/insulator-hybrid isolation for self-powered wearable devices. *IEEE Transactions on Electron Devices, 67*(9), 3834–3842.
16. Chen, J., Klein, J., Wu, Y.-J., Xing, S.-X., Flammang, R., Heibel, M., & Zuo, L. (2016). A thermoelectric energy harvesting system for powering wireless sensors in nuclear power plants. *IEEE Transactions on Nuclear Science, 63*(5), 2738–2746.
17. Yang, B., Zhang, M.-T., Wang, J.-B., Zeng, K.-D., Zhang, Z.-A., Shu, H.-C., Zhang, X.-S., & Yu, T. (2021). Interacted collective intelligence based energy harvesting of centralized thermoelectric generation systems under non-uniform temperature gradient. *Sustainable Energy Technologies and Assessments, 48*, 101600.
18. Liu, Y.-H., Chiu, Y.-H., Huang, J.-W., & Wang, S.-C. (2016). A novel maximum power point tracker for thermoelectric generation system. *Renewable Energy, 97*, 306–318.
19. Zhang, X.-S., Yang, B., Yu, T., & Jiang, L. (2020). Dynamic surrogate model based optimization for mppt of centralized thermoelectric generation systems under heterogeneous temperature difference. *IEEE Transactions on Energy Conversion, 35*(2), 966–976.
20. Bijukumar, B., Raam, A. G. K., Ganesan, S. I., & Nagamani, C. (2018). A linear extrapolation-based MPPT algorithm for thermoelectric generators under dynamically varying temperature conditions. *IEEE Transactions on Energy Conversion, 33*(4), 1641–1649.
21. Twaha, S., Zhu, J., Yan, Y.-Y., Li, B., & Huang, K. (2017). Performance analysis of thermoelectric generator using dc–dc converter with incremental conductance based maximum power point tracking. *Energy for Sustainable Development, 37*, 86–98.
22. Mansoor, M., Mirza, A. F., Duan, S.-H., Zhu, J., Yin, B.-Q., & Ling, Q. (2021). Maximum energy harvesting of centralized thermoelectric power generation systems with non-uniform temperature distribution based

on novel equilibrium optimizer. *Energy Conversion and Management, 246*, 114694.
23. Yang, B., Wang, J.-T., Zhang, X.-S., Zhang, M.-T., Shu, H.-C., Li, S.-N., He, T.-Y., Yang, L., & Yu, T. (2019). MPPT design of centralized thermoelectric generation system using adaptive compass search under non-uniform temperature distribution condition. *Energy Conversion and Management, 199*, 111991.
24. Mirza, A. F., Mansoor, M., Zerbakht, K., Javed, M. Y., Zafar, M. H., & Khan, N. M. (2021). High-efficiency hybrid PV-TEG system with intelligent control to harvest maximum energy under various non-static operating conditions. *Journal of Cleaner Production, 320*, 128643.
25. Li, F.-S., Lin, D., Yu, T., Li, J.-W., Wang, K.-Y., Zhang, X. S., Yang, B., & Wu, Y.-F. (2021). Adaptive rapid neural optimization: A data-driven approach to MPPT for centralized TEG systems. *Electric Power Systems Research, 199*, 107426.
26. Chen, M. (2014). Adaptive removal and revival of underheated thermoelectric generation modules. *IEEE Transactions on Industrial Electronics, 61*(11), 6100–6107.
27. Belhachat, F., & Larbes, C. (2021). PV array reconfiguration techniques for maximum power optimization under partial shading conditions: A review. *Solar Energy, 230*, 558–582.
28. Yang, B., Ye, H.-Y., Wang, J.-B., Li, J.-L., Wu, S.-C., Li, Y.-L., Shu, H.-C., Ren, Y.-X., & Ye, H. (2021). PV arrays reconfiguration for partial shading mitigation: Recent advances, challenges and perspectives. *Energy Conversion and Management, 247*, 114738.
29. Aljafari, B., Satpathy, P. R., & Thanikanti, S. B. (2022). Partial shading mitigation in PV arrays through dragonfly algorithm based dynamic reconfiguration. *Energy, 257*, 124795. https://doi.org/10.1016/j.energy.2022.124795
30. Pachauri, R. K., Thanikanti, S. B., Bai, J., Yadav, V. K., Aljafari, B., Ghosh, S., & Alhelou, H. H. (2022). Ancient Chinese magic square-based PV array reconfiguration methodology to reduce power loss under partial shading conditions. *Energy Conversion and Management, 253*, 115148.
31. Reddy, S. S., & Yammani, C. (2020). A novel Magic-Square puzzle based one-time PV reconfiguration technique to mitigate mismatch power loss under various partial shading conditions. *Optik, 222*, 165289.
32. Zhang, X.-S., Li, C.-Z., Li, Z.-L., Yin, X.-Q., Yang, B., Gan, L.-X., & Yu, T. (2021). Optimal mileage-based PV array reconfiguration using swarm reinforcement learning. *Energy Conversion and Management, 232*, 113892.
33. Chen, M. (2014). Reconfiguration of sustainable thermoelectric generation using wireless sensor network. *IEEE Transactions on Industrial Electronics, 61*(6), 2776–2783.
34. Zhang, X.-S., Tan, T., Yang, B., Wang, J.-B., Li, S.-N., He, T.-Y., Yang, L., Yu, T., & Sun, L.-M. (2020). Greedy search based data-driven algorithm of centralized thermoelectric generation system under non-uniform temperature distribution. *Applied Energy, 260*, 114232.
35. Chakraborty, A., Saha, B. B., Koyama, S., & Ng, K. C. (2006). Thermodynamic modelling of a solid state thermoelectric cooling device: Temperature-entropy analysis. *International Journal of Heat and Mass Transfer, 49*(19–20), 3547–3554.
36. Han, H. S., Kim, Y. H., Kim, S. Y., Um, S., & Hyun, J. M. (2010). Performance measurement and analysis of a thermoelectric power generator. In *IEEE intersociety conference on thermal thermomechanical phenomena electronics systems*, Las Vegas, NV, USA, pp. 1–7.
37. Kong, C.-S. (1995). A general maximum power transfer theorem. *IEEE Transactions on Education, 38*(3), 296–298.
38. Glover, F. (1989). Tabu search-part I. *INFORMS Journal on Computing, 1*(3), 190–206.
39. Glover, F. (1990). Tabu search-part II. *INFORMS Journal on Computing, 2*(1), 4–32.
40. Trojovský, P., & Mohammad, D. (2022). Pelican optimization algorithm: A novel nature-inspired algorithm for engineering applications. *Sensors, 22*(3), 855.
41. Ding, H., Sun, G.-Y., Hao, L.-J., Wu, B., & Wu, Y.-C. (2020). A loading pattern optimization method based on discrete differential evolution. *Annals of Nuclear Energy, 137*, 107057.
42. Zhang, Y.-J., Li, T., Na, G.-Y., Li, G.-Q., & Li, Y. (2015). Optimized extreme learning machine for power system transient stability prediction using synchrophasors. *Mathematical Problems in Engineering, 2015*, 529724.
43. Gu, X.-P., Li, Y., & Jia, J.-H. (2015). Feature selection for transient stability assessment based on kernelized fuzzy rough sets and memetic algorithm. *International Journal of Electrical Power & Energy Systems, 64*, 664–670.
44. Karaboga, D., & Ozturk, C. (2011). A novel clustering approach: Artificial bee colony (ABC) algorithm. *Applied Soft Computing, 11*(1), 652–657.
45. Dorigo, M., Birattari, M., & Stutzle, T. (2006). Ant colony optimization. *IEEE Computational Intelligence Magazine, 1*(4), 28–39.